

**Fused Deposition Modeling (FDM)
Material Properties Characterization**

ME 222 Final Project

John Michael Brock
Michael Montero
Dan Odell
Shad Roundy

Spring Semester
May 5, 2000

1.0 Introduction

Recent advances in the fields of Computer Aided Drafting (CAD) and Rapid Prototyping (RP) have given designers the tools to rapidly generate an initial prototype from a concept. There are currently several different RP technologies available, each with its own unique set of competencies and limitations. In this paper, we seek to characterize some of the properties of Stratasys' Fused Deposition Modeling (FDM) process, as well as the effects of varying some of the build parameters.

Before we can discuss the properties of an FDM part, we must first discuss how the process works. The first step in generating an FDM part is to create a three dimensional solid model. This can be accomplished in many of the commonly available CAD packages. The part is then exported to the FDM Quickslice™ software via the stereolithography (STL) format. This format reduces the part to a set of triangles by tessellating it. The advantage of this is that it is a common format that almost every CAD system can export, and reduces the part to its most basic components. The disadvantage is that the part loses some resolution, as only triangles, and not true arcs, splines, etc now represent it. However, these approximations are acceptable as long as they are less than the inaccuracy inherent in the manufacturing process.

Once the STL file has been exported to Quickslice™, it is then horizontally sliced into many thin sections. These sections represent the two dimensional contours that the FDM process will generate which, when stacked upon one another, will closely resemble the original part three dimensional part. This sectioning approach is common to all currently available Rapid Prototyping processes. Obviously, the thinner the sections, the more accurate the part. The software then uses this information to generate the process plan that controls the FDM machine's hardware.

FDM

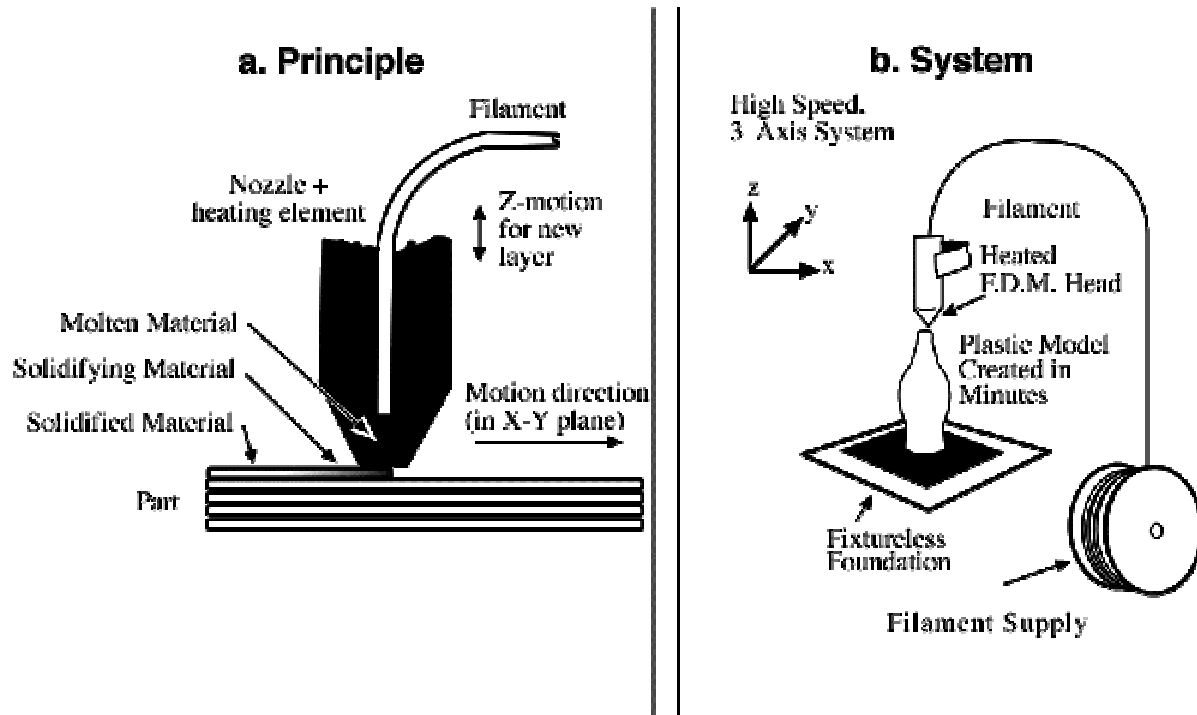


Figure 1.1 Fuse deposition modeling process.

The Hardware for the FDM machine is represented in Figure 1.1. The concept is that a filament, in our case ABS, is fed through a heating element, which heats it to a molten state. The filament is then fed through a nozzle and deposited onto the part it is building. This aspect is not unlike squeezing toothpaste from a tube. Since the material is extruded in a molten state, it fuses with the material around it that has already been deposited. The head is then moved around in the X-Y plane and deposits material according to the part requirements from the STL file. The head is then moved vertically in the Z plane to begin depositing a new layer when the previous one is completed. After a period of time, usually several hours, the head will have deposited a full physical representation of the original CAD file.

It is interesting to note that this approach may require a support structure to be built beneath the sections. If one horizontal slice overhangs the one below, it will simply fall to the substrate when the FDM nozzle attempts to deposit it. The FDM machine possesses a second nozzle that

extrudes support material for this purpose. The support material is similar to the model material, but it is more brittle so that it may be easily removed after the model is completed. The FDM machine builds support for any structure that has an overhang angle of less than 45° from horizontal. If the angle is less than 45°, more than one half of one bead is overhanging the slice below it, and therefore is likely to fall.

This process results in a part with unique characteristics. While it is much tougher than parts made by other RP processes (such as SLA), we have still experienced brittle fractures at relatively low loads. This experience goes against the blanket claim that Stratasys makes that FDM parts possess 70% of the strength of solid ABS parts. Also, this claim is very vague as the yield strength of ABS can vary from 29 MPa to 124 MPa. In addition, it is very clear that the FDM process deposits material in a direction way, which results in non-isotropic parts. With these problems in mind, we set out to characterize the material behavior of FDM parts, as well as the effects of some of the process control parameters.

2.0 Build Parameter Considerations

To begin our experiment, we first identified the process control parameters that were likely to affect the properties of FDM parts. The parameters we selected are listed below:

Bead (or road) width: This is the thickness of the bead (or road) that the FDM nozzle deposits. It can vary from .012” to .0396” for the T12 nozzle which is currently installed on our Stratasys™ FDM 1650 machine.

Air Gap: This is the space between the beads of FDM material. The default is zero, meaning that the beads just touch. It can be modified to leave a positive gap, which means that the beads of material do not touch. This results in a loosely packed structure that builds rapidly. It can also be modified to leave a negative gap, meaning that two beads partially occupy the same space. This results in a dense structure which requires a longer build time.

Model Build Temperature: The temperature of the heating element for the model material. This controls how molten the material is as it is extruded from the nozzle.

Raster Orientation: The direction of the beads of material (roads) relative to the loading of the part.

Color: FDM ABS material is available in a variety of colors: white, blue, black, yellow, green, and red.

We decided to neglect the possible affects of envelope temperature (the temperature of the air around the part), slice height (which is similar to bead width in the vertical direction), and nozzle diameter (the width of the hole through which the material extrudes). These parameters seemed either duplicates of parameters we selected, or did not seem to have a relevant connection to the final material properties.

3.0 Experiment Setup

To begin testing, we built a series of samples on the FDM machine (see Design of Experiment section for more detail). Examples of test parts can be seen in Figures 3.1 (Quickslice views of parts) and 3.2 (actual test specimens with loading directions indicated). Note that the loading directions in Figure 3.2 define the terminology that will be used throughout the remainder of this paper.

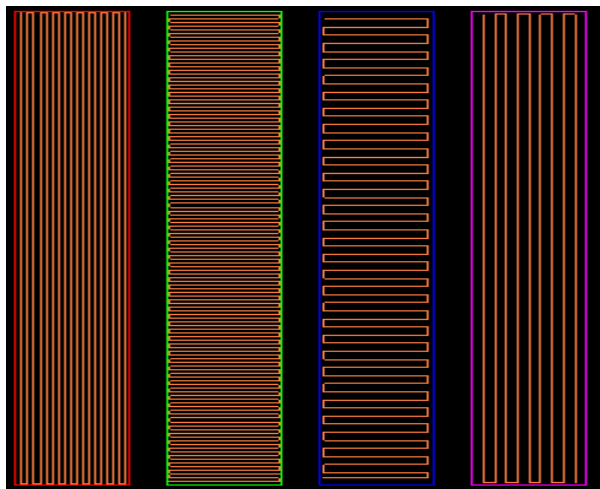


Figure 3.1 Quickslice SML file showing samples with bead-width, air gap, and raster orientation variation.

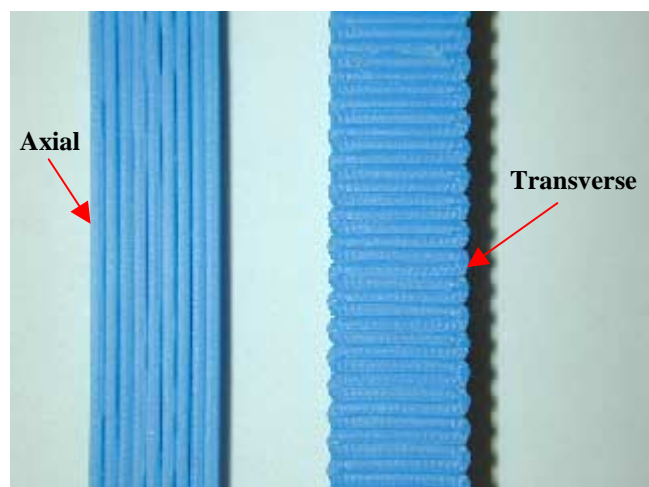


Figure 3.2 Actual tensile specimens in axial (1) and transverse (2) load directions

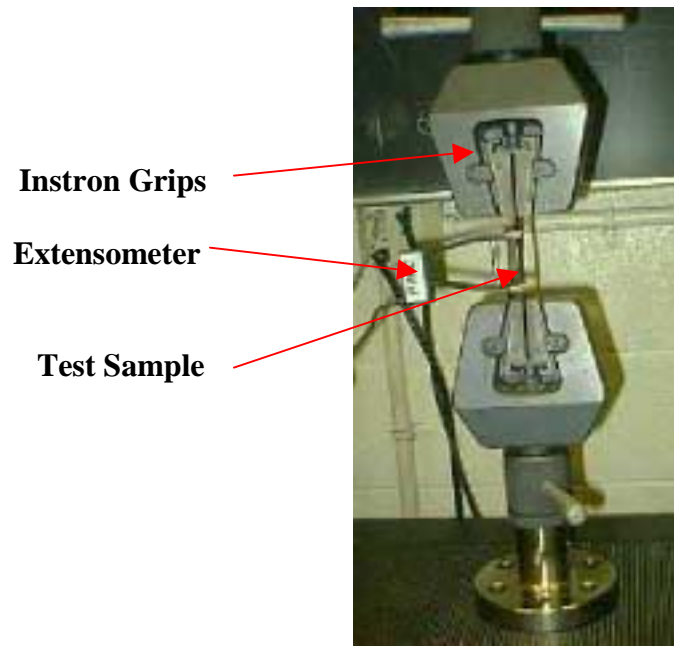


Figure 3.3 Instron load frame set-up.

To test the properties of our test samples, we used an Instron load frame to load the samples in tension. We then collected the load and extension data of the sample as it was loaded. To measure the strain of our sample, we used an extensometer (see Figure 3.3). This device limited our max test strain to twenty percent. As the extensometer only measures strain between its blades, we also collected displacement data at the grips for comparison.

When we began our testing, we used samples that conformed to the ASTM D-638 97, type I standard (a dog-bone shaped sample). However, we quickly ran into problems with this approach. As you can see in Figures 3.4 and 3.5, the dog-bone shape added complications to the loading of the parts that caused them to fail pre-maturely. We attempted to use two different approaches with this shape: a raster approach, and a contour approach. The raster approach yielded a series of infinitely small stress concentrations at the site of what was supposed to be a large, stress concentration reducing, three-inch radius. The contour approach yielded stress-concentrating gaps in the middle of the part, as well as a non-axial stress state at the radii. While the contours were better than the rasters, we decided to abandon the dog-bone shape in favor of a simple rectangle that possessed no potential stress concentrators at all. We landed on a sample

size of Width .375" x Length 4.00" x Thickness .125" for axial samples, and a thickness of .25" with the same width and length for our transverse samples.



Figure 3.4 Trouble with stress concentration - 3" radius actually infinitely small.

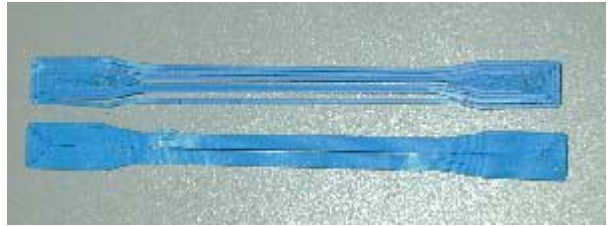


Figure 3.5 Trouble with contours - Gaps, stress concentration, and (2) loading.

4.0 Design of Experiment (DOE)

The goal of the experiment is to see how changing multiple design and process variables effects tensile strength within FDM tensile specimens. As mentioned before, the actual variables selected for the experiment are chosen from a larger set based on intuitive knowledge of each parameter. Figure 4.1 shows the larger set of variables and under what domain or classification they fall under.

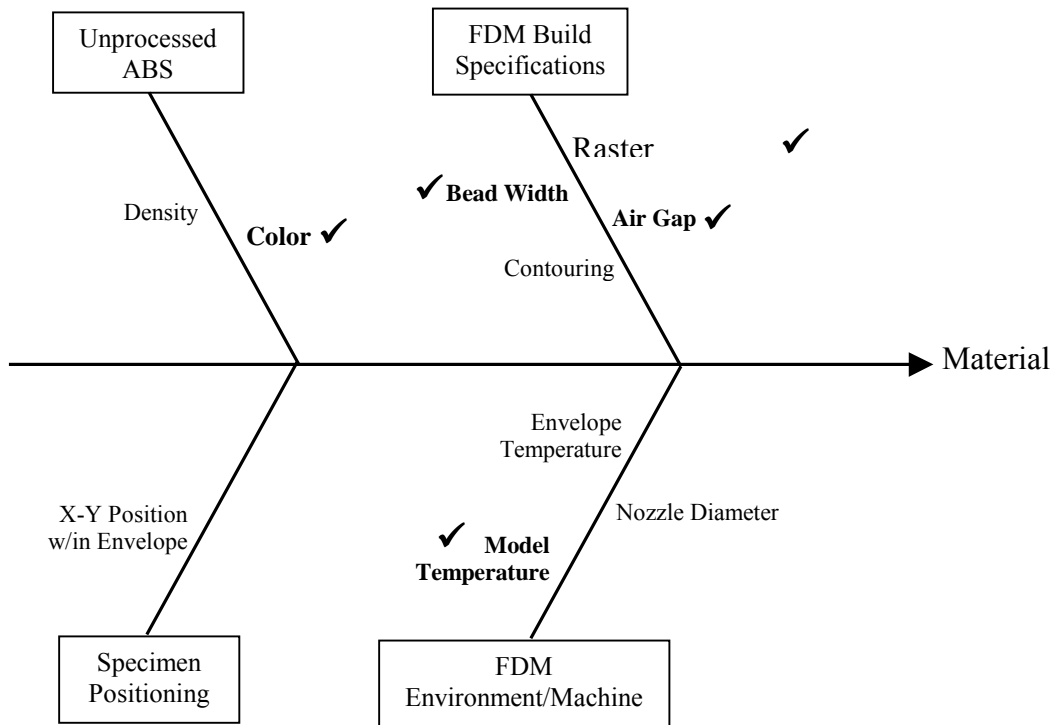


Figure 4.1 Fishbone diagram of potential factors influencing tensile strength

The five variables selected are actually from three different classifications: unprocessed ABS, FDM build specifications, and FDM environment. The five variables are air gap, bead width, model temperature, ABS color, and raster orientation. Amongst the five variables, one variable is qualitative (ABS color) whereas the remaining four are quantitative parameters. The next step in the setup of the DOE is to determine the type of resolution for the experiment and the number of levels for each variable.

The experiment should yield unambiguous results between the estimation of variable effects as well as be conducted within a reasonable amount of time. Build time for each tensile specimen is taken into consideration as well as the time needed to perform the fracture test. Therefore, minimizing the number of tests within the experiment while providing clear estimations of the effects are the highest of priority. Keeping that in mind, a fractional factorial DOE is selected to meet both requirements.

We hope to see a linear behavior of the response (tensile strength) as a function of the 5 variables. For that reason, each parameter will have two levels set at a high (+1) and a low (-1). In order to set the appropriate levels for each variable, preliminary tests were conducted for each variable to define its range. Each variable was varied independently from all the others and the tensile strength was measured. The results of these preliminary tests gave us a suitable range for the two levels of each parameter. Figure 4.2 shows the parameters, their associated symbols, and their level settings.

Variable	Symbol	Levels	
		Low(-)	High(+)
Air Gap (in.)	A	0.0000	-0.0020
Road Width (in.)	B	0.02	0.0396
Model Temperature (C)	C	270	280
ABS Color	D	Blue	White
Orientation of Rasters	E	Transverse	Axial

Figure 4.2 Variable symbols and level settings.

By only having two levels, a 2^{5-1} design will provide a high-resolution (V) and only 16 required test conditions. The resolution of the design is an indicator of the degree of confounding within the effect estimations for each variable. Confounding is the inability to distinguish one variable effect from another. With a resolution V design, we will have 16 estimates of effects whereby the main effects are confounded with 4-factor interactions and 2-factor interactions are confounded with 3-factor interactions. The resolution number represents the smallest word within the defining relation of a design. The defining relation is used to determine which effects are confounded with each other. In order to obtain a defining relation, a generator is needed and can be selected from the possible combinations of variables. In our design, variable E (or raster

orientation) will be our generator. We choose $E = ABCD$ and from our generator we can obtain our defining relation by simply multiplying each side by E . Therefore, the defining relation is the following: $I = ABCDE$. We can now multiply all main effects and multi-factor interaction effects by the defining relation to reveal the confounding terms within each effect estimate. Figure 4.3 shows the following process of obtaining a resolution V DOE.

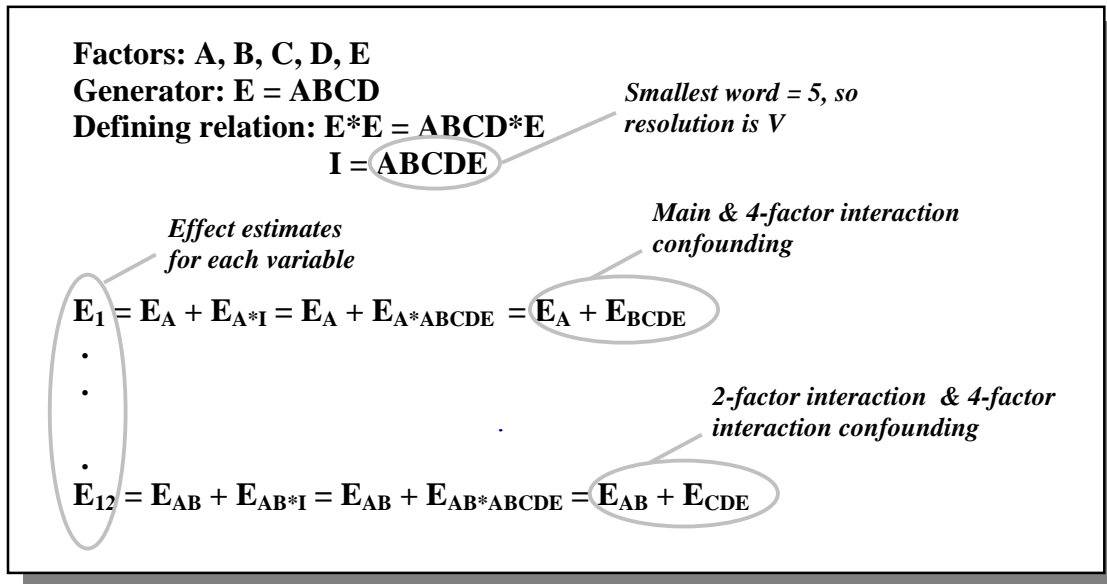


Figure 4.3 Defining effect estimates using defining relation for resolution V DOE.

Not only does the generator and defining relation help deriving the effect estimates, but they also help in setting the appropriate test conditions for the design matrix. Since our generator is $E = ABCD$, then the test conditions for parameter E will be defined by the product of coded units (+1 and -1) of columns $A, B, C,$ and D . Figure 4.4 shows the design matrix. With only 16 test conditions, it was decided to replicate each one in order to calculate an estimate of the standard error within our experiment. The variance calculated will be used in conjunction with the *student-t* distribution to produce confidence intervals ($\alpha = 97.5\%$) of each effect estimate to verify statistical significance. The final design contains a total of 32 test specimens, which is an advantage over a full factorial design (2^5) which contains the same number of runs but lacks the estimate of error. The following section shows the results of the DOE but does not go deep into the computation of the effects. Further details can be found in Box and Hunter's *Statistics for Experimenters*.

Test No.	Variables					Response (MPa)		
	A	B	C	D	E	Y_1	Y_2	Y_AVE
1	-1	-1	-1	-1	1	y1_1	y1_2	y1_av
2	1	-1	-1	-1	-1	y2_1	y2_2	y2_av
3	-1	1	-1	-1	-1	y3_1	y3_2	y3_av
4	1	1	-1	-1	1	y4_1	y4_2	y4_av
5	-1	-1	1	-1	-1	y5_1	y5_2	y5_av
6	1	-1	1	-1	1	y6_1	y6_2	y6_av
7	-1	1	1	-1	1	y7_1	y7_2	y7_av
8	1	1	1	-1	-1	y8_1	y8_2	y8_av
9	-1	-1	-1	1	-1	y9_1	y9_2	y9_av
10	1	-1	-1	1	1	y10_1	y10_2	y10_av
11	-1	1	-1	1	1	y11_1	y11_2	y11_av
12	1	1	-1	1	-1	y12_1	y12_2	y12_av
13	-1	-1	1	1	1	y13_1	y13_2	y13_av
14	1	-1	1	1	-1	y14_1	y14_2	y14_av
15	-1	1	1	1	-1	y15_1	y15_2	y15_av
16	1	1	1	1	1	y16_1	y16_2	y16_av

Figure 4.4 2^{5-1} design matrix with 2 response replicates

5.0 Analysis of DOE

Figure 5.1 shows the tensile strengths for each test condition with 2 replicates. The average response was used in calculating all 16 effects. The variance among the responses within each test was calculated. Tests 2, 3, 5, 9, and 12 show large variations and can be contributed to the random defects which exist between layers of the tensile specimen. These random defects make the bulk specimen susceptible to stress concentrations especially when raster orientation (E) is traverse (-1). These large variations may inflate the overall effect variance.

Test	A	B	C	D	E	Y ₁ (MPa)	Y ₂ (MPa)	Y _{AVE}	R	s _i ²	DOF
1	-1	-1	-1	-1	1	19.17	20.02	19.60	-0.85	0.36	1
2	1	-1	-1	-1	-1	10.00	14.08	12.04	-4.08	8.32	1
3	-1	1	-1	-1	-1	1.14	2.96	2.05	-1.82	1.65	1
4	1	1	-1	-1	1	22.77	23.20	22.98	-0.42	0.09	1
5	-1	-1	1	-1	-1	3.40	1.54	2.47	1.86	1.73	1
6	1	-1	1	-1	1	21.57	21.42	21.50	0.15	0.01	1
7	-1	1	1	-1	1	20.93	20.48	20.71	0.45	0.10	1
8	1	1	1	-1	-1	11.38	10.98	11.18	0.40	0.08	1
9	-1	-1	-1	1	-1	1.42	3.17	2.30	-1.75	1.53	1
10	1	-1	-1	1	1	22.99	22.50	22.74	0.50	0.12	1
11	-1	1	-1	1	1	20.77	21.39	21.08	-0.63	0.20	1
12	1	1	-1	1	-1	5.42	8.18	6.80	-2.77	3.83	1
13	-1	-1	1	1	1	20.27	19.90	20.08	0.37	0.07	1
14	1	-1	1	1	-1	12.07	12.92	12.50	-0.85	0.36	1
15	-1	1	1	1	-1	0.90	1.98	1.44	-1.08	0.59	1
16	1	1	1	1	1	23.50	23.30	23.40	0.20	0.02	1

Figure 5.1 DOE responses, average responses, ranges, test variances, and degrees of freedom

Figure 5.2 shows the estimates of effects. Since 3-factor interactions or higher have a low probability of occurring (or showing large effects) due to the nature of the FDM machine, we assume that they are negligible. This assumption may not hold true and is highly dependent on the mechanism under questions. For instance, DOE's that investigate chemical compositions will include higher order interactions since the nature of the mechanism presents a higher probability of yielding significant higher order interactions. Keeping that in mind, Figure 5.2 shows how each effect can be resolved or essentially three-factor or higher interactions can be removed from the estimate.

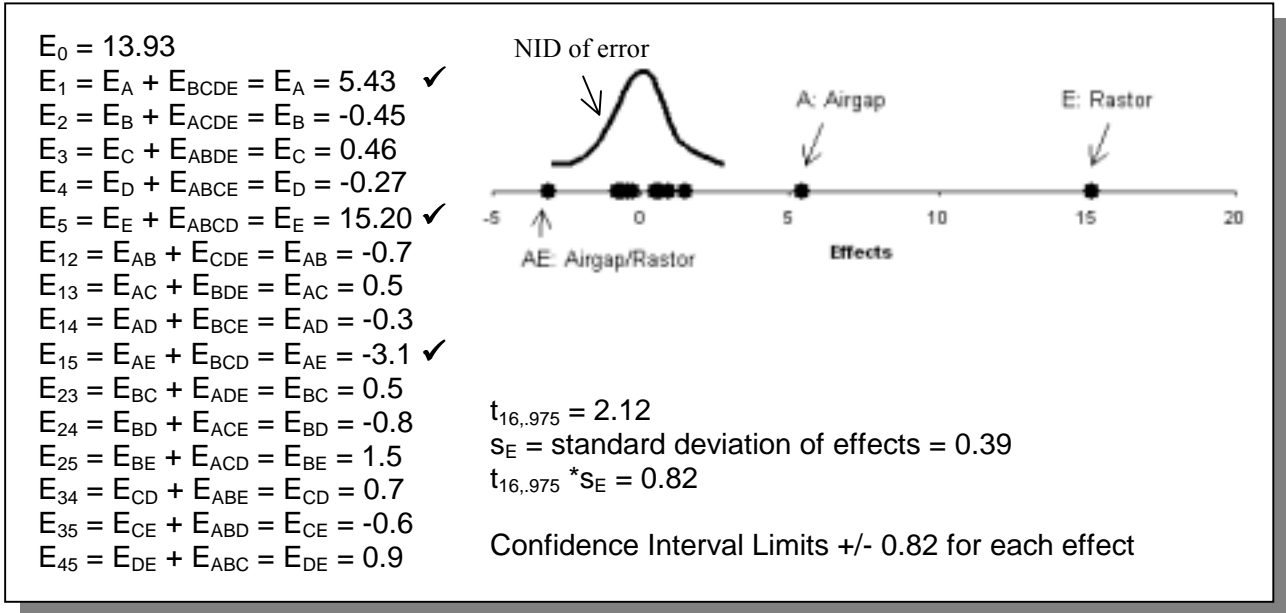


Figure 5.2 Effect results, dot plot of effects, and confidence interval limits shown.

Figure 5.2 shows that variables A, E and the interaction AE had a significant effect on the tenile strength response. The confidence interval limits calculated were used to verify statistical significance of the effect. The limit plus the effect gives a range of the effect and if 0 is encompassed within the range, the effect is considered null or not significant. In the case of E_{45} , the effect is on the fringes of the interval and was still considered null. A visual representation of the main effects can be seen in Figure 5.3. It is clear that air gap and raster orientation when set from low to high levels have a significant effect by increasing the tensile strength.

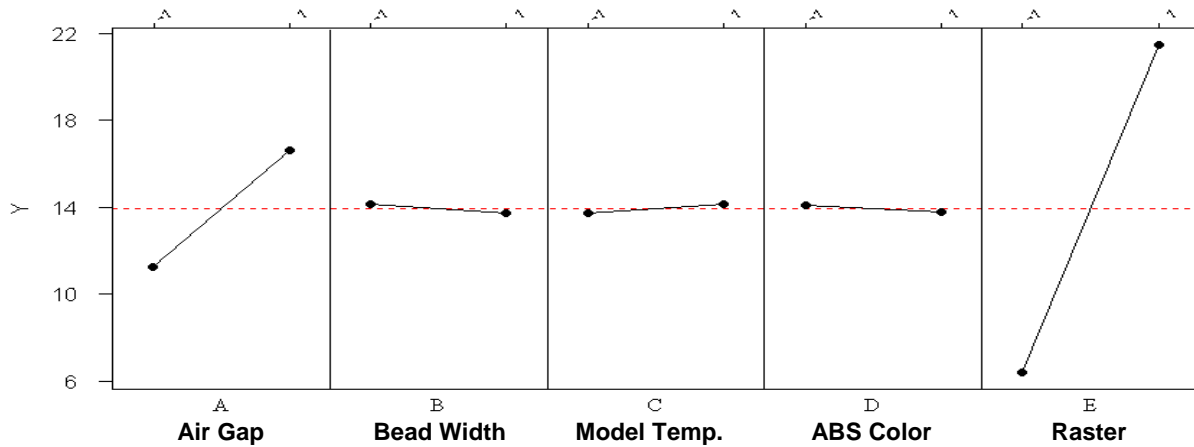


Figure 5.3 Plot of tensile strength versus main effects.

If we look at the effect of AE on tensile strength in Figure 5.4, a strong interaction between both variables exists. When the tensile specimen has the roads oriented in the traverse direction (-1) the air gap will influence the tensile strength greatly. On the other hand, when the roads are oriented axially (+1), the air gap effect is less.

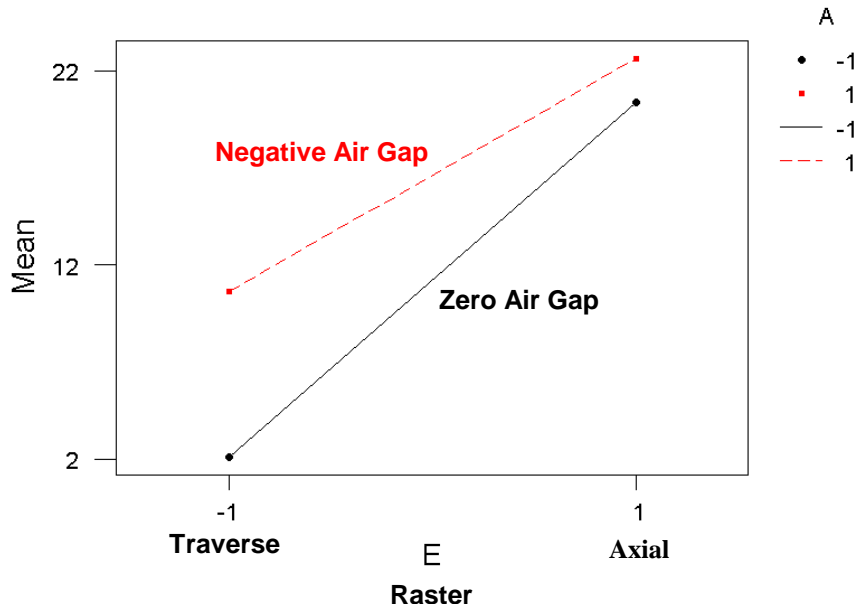


Figure 5.4 Interaction plot of tensile strength versus air gap/raster interaction.

6.0 Predictive Model from DOE

The DOE not only determines which effects are significant, but it also formulates a mathematical model using the effects as coefficients for the significant variables. The following formula (1) shows tensile strength as a function of air gap and raster orientation.

$$y = \text{tensile strength} = 13.9 + 2.7A + 7.6E - 1.6A * E \quad (1)$$

The model can be used to interpolate values or extrapolate. Further experiments utilize the model to eventually construct a surface response in order to find an optimum. We decided to use the model as a method of predicting tensile strengths by conducting four additional tests. The test levels and results are shown in Table 6.1. The model holds up well when raster orientation is held axially and air gap is varied in Test 1 and 2. The error for Test 1 and 2 are 6.3 % and 4.4%

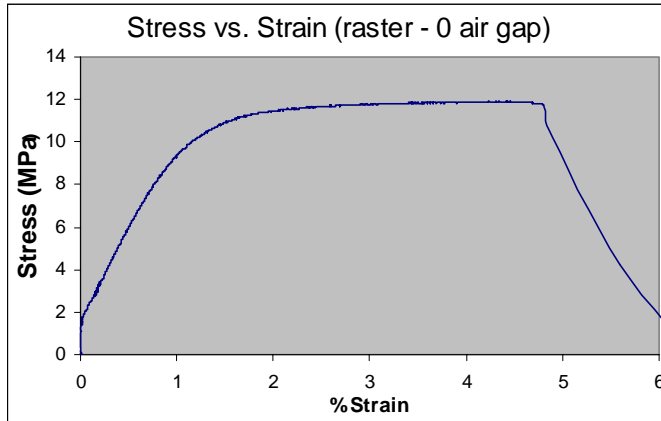
respectively. On the other hand, the model does not hold up well for Test 3 showing a large error between the tensile strengths. During actual fracture test, the tensile specimen for Test 3 appeared to have a defect present within the layers of the material. During the tensile test, the specimen fractured in the region of the defect very quickly with very little strain. The large error in Test 3 could be attributed to this initial defect present. Test 4 yields reasonably close tensile strengths between the predictive and experimental values with an error of 6.2 %.

Test No.	A: Air Gap (in.)	E: Raster (orient.)	Predictive Tensile Strength (MPa)	Experimental Tensile Strength (MPa)
1	0.000	Axial	20.4	19.2
2	-0.001	Axial	21.5	20.6
3	0.000	45°	11.2	3.3
4	-0.001	45°	16.6	17.7

Table 6.1 Predictive model versus experimental results

7.0 Further Analysis

In practice, most FDM parts are made with a crisscross raster in which the orientation of the beads alternates from +45° to -45° from layer to layer. Some crisscross raster specimens were built and tested in addition to the main factorial experiment. The two purposes for these tests were first to test whether the results for the main factorial experiment hold for a crisscross raster,



	Y(measured)	Y(predicted)
Zero Air Gap	11.7 MPa	11.2 MPa
-.002 in. Air Gap	18.2 Mpa	16.6 MPa

Figure (7.1)

and second to verify the predictive model, which will be explained in detail later. An example stress vs. strain curve for these tests is shown in Figure (7.1). Notice that there is a significant amount of plastic behavior for these parts. The factorial experiment indicated that the only two significant factors are raster orientation and air gap. Since the raster orientation is already set for a crisscross raster, the only factor varied for these tests was air gap. As shown in Figure

(5.1), the parts with a negative air gap are significantly stronger. Also, the tensile strength predicted by the model from the factorial experiment matches the actual data reasonably well.

The elastic modulus was measured for the parts that were tested as part of the factorial experiment and for the crisscross raster parts. These results are summarized in Table (7.1). The

	Axial	Transverse	Crisscross 0 Air Gap	Crisscross -.002 Air Gap
E (GPa)	1.6	1.0	1.48	0.8

Table (7.1)

parts built with an axial raster orientation were significantly more stiff than those built with transverse raster orientation. Also, the crisscross raster parts with a negative air gap were more stiff than those built with zero air gap. Interestingly, air gap did not have a significant effect on the elastic modulus for the axial or transverse parts. Bulk ABS has an elastic modulus of about 2 GPa, or about twice that of the FDM parts built out of ABS. Figure (7.2) shows a stress vs. strain curve for part built with axial rasters. Notice the sharp peak at the end of the elastic region

and the significant perfectly plastic behavior. Almost all of the axial parts exhibited large plastic strains similar to the one shown here.

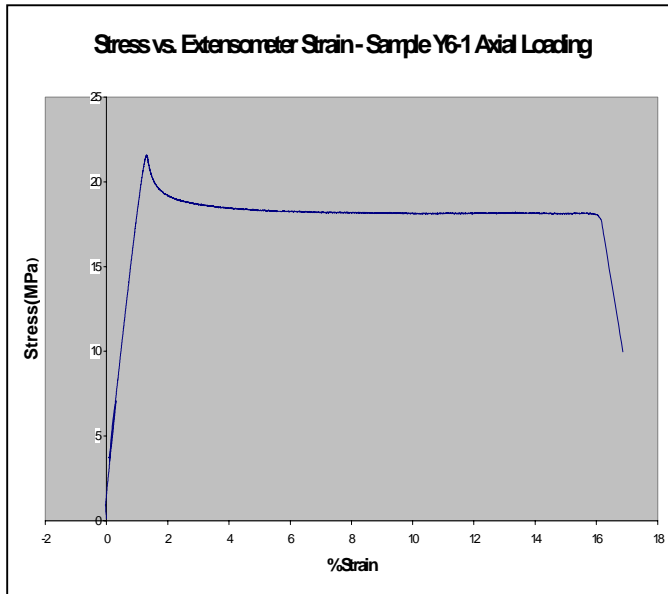


Figure (7.2)

Some parts reached strains of 18%, which was the maximum strain to which the Instron machine would extend. The average stress value of the flat part of this stress strain curve is 18 MPa.

Finally some shear specimens as shown in Figure (A.4) in the Appendix were tested. As explained, the FDM builds parts layer by layer. Each layer is created using beads (or roads) or

extruded ABS plastic. So, shear specimens were built to test the shear strength and modulus between both roads and layers. The results of these tests are shown in Table (7.2). The specimens were both stronger and stiffer between layers than between roads.

	E_{sh} (GPa)	S (MPa)
Between Layers	1.41	10.03
Between Roads	0.69	7.35

Table (7.2)

8.0 Classical Plate Theory

Classical plate theory applies to bodies for which one dimension is significantly smaller than the other two. Several assumptions about the deformation of such a body are made. The displacement in the z -direction, w , of a point is assumed to be independent of its z -position. Further, the displacement of a point in the x -direction, u , (or y -direction, v) is assumed to be the sum of the midplane displacement and the distance from the midplane multiplied by the slope of the midplane. In other words, plane sections remain plane and normals remain normal.

A critical aspect of classical plate theory is seen when strain-displacement relations are applied to the above displacement assumptions. The result is that all components of strain in the z -direction, the normal and transverse shear strains, are zero. That means that all loads are carried by in plane stresses, including loads applied in the z -direction. Integrating the in plane stresses over the thickness of the plate, z , gives the applied loads in the x - and y -directions. If the in plane normal and shear stresses are multiplied by their z position and then integrated the applied moments are found. With these relations, measured quantities, forces and displacements, can be related to stresses and strains, which in practice are hard to measure.

8.1 Laminated Plate Theory

Laminated plate theory extends classical plate theory for bodies that are comprised of layers, called plies, which may or may not have similar properties. The theory is generally applied to materials that are either orthotropic or transversely isotropic. Consequently the material properties of the body may not be uniform throughout the thickness, instead just throughout each layer. Laminated plate theory only considers the material properties of a plate as a whole. For a composite, where the layers are comprised of fibers and matrix, the bulk behavior of the composite is only of interest. For orthotropic and transversely isotropic materials the properties are a function of orientation of the ply. A ply coordinate system is defined with the 1-direction aligned with the direction of maximum stiffness, and the 2-direction rotated 90 degrees in plane. To determine the properties in body coordinates of an arbitrarily oriented ply, a fourth order tensor rotation of the plane strain reduced stiffness matrix is performed.

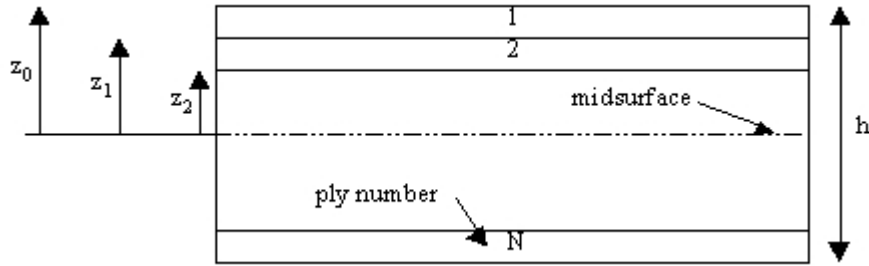


Figure 8.1 Book-keeping scheme of ply properties and positions. [1]

Just as was discussed in classical plate theory, the external moments and forces that cause stresses in the plate are found by integrating the stresses over the stresses multiplied by their vertical position over the thickness, respectively. An assumption is made that there is perfect bonding between all layers of the composite, and as a result the strain is continuous throughout the thickness. Because the material properties are only piecewise constant throughout the thickness, the stresses can be discontinuous at the interfaces between layers. Therefore the integration must be broken up and performed layer by layer. The stress is found by multiplying the reduced stiffness matrix in body coordinates of each ply by the midplane strain of each ply. As previously mentioned the midply strain is the sum of the midplane strain and the effect of rotation of the midplane. The sum of the integrals is equal to the externally applied loads.

However, the external loads that will be applied to a body are usually known while the displacements and hence stress and strain are unknown. If the above analysis is inverted, the midplane strains and curvatures are equal to the inverted plane strain reduced stiffness matrices multiplied by the force matrix. From the midplane strains and curvatures the midply strains in body coordinates can be deduced. Multiplying by the plane strain reduced stiffness gives the midply stress for each ply. Using second order tensor rotations, the stresses and strains in the ply coordinates are determined.

8.2 Tsai Wu Failure Criterion

Tsai Wu Failure Criterion is used to predict yield in orthotropic materials. It is a relation that was developed from empirical data based upon failure of hundreds of materials. The hypothesis is that a material fails when the ratio of applied stress to yield strength is equal to one. Tsai Wu

accounts for a three-dimensional state of stress and anisotropic yield strengths. Failure occurs when,

$$F_{11}\sigma_1^2 + 2F_{12}\sigma_1\sigma_2 + F_{22}\sigma_2^2 + F_{66}\sigma_6^2 + F_1\sigma_1 + F_2\sigma_2 = 1 \quad (2)$$

$$F_{11} = \frac{1}{X_c X_t}; \quad F_1 = \frac{1}{X_c} - \frac{1}{X_t}; \quad F_{22} = \frac{1}{Y_c Y_t}; \quad F_2 = \frac{1}{Y_t} - \frac{1}{Y_c}; \quad F_{66} = \frac{1}{S^2}; \quad F_{12} = 0 \quad (3)$$

X_c and X_t are the yield strengths in compression and tension respectively in the x-direction. Y_c and Y_t are the yield strengths in the y-direction, and S is the yield strength in shear.

9.0 Laminated Plate Predictive Model

Thus far we have discussed the behavior of FDM material in the axial and transverse directions. In practice, a part rarely has all of the beads aligned in a single direction. In fact, the default setting of Stratasys' Quickslice program alternates the direction of the beads by 90 degrees between each layer. Overwriting the default values makes it possible to specify an orientation for each individual layer. The sequence of orientations is known as the stacking sequence, or layup. Using laminated plate theory, two Matlab programs were written to predict the behavior of a part with arbitrary layup.

In the first program, **lam.m**, the user specifies the layup of the material and the loading scenario. The possible loads are axial forces in the x- and y-directions, an in plane shear force, moments about the x- and y-direction and an in plane twisting moment. It is important to note that the x- and y-directions refer to the coordinate system of the part, not the coordinate system of any particular layer. The program will calculate and output: the reduced stiffness matrix in part coordinates, the laminate stiffness matrix, the midplane strains and curvatures, the strains and stresses in part coordinates and layer coordinates, and the Tsai Wu failure results. This program is useful for applying multiple loads and observing the laminate stiffness matrix, the strains and failure results. A second program, **fail.m**, uses much the same architecture as the **lam.m** but will predict the maximum load in any one direction the laminate can withstand. It does so by entering a while loop that will recursively increase the load until failure of a single ply is

observed with a resolution of one hundredth of a MPa. This program is useful for determining the load at which a part will fail if the layup and loading direction are known but the magnitude of the loading is unknown.

9.1 Results

The accuracy of the programs was tested by comparing predicted behavior with actual behavior measured in an Instron machine using two loading scenarios. In the first case, two samples, one with zero air gap and one with -0.002" air gap, with repeating 45°, -45° layup were pulled in tension until they failed. The purpose of this experiment was to determine if **fail.m** would predict the correct failure load for a part with non-uniform layup. In the second test two strips were built with symmetric but opposite layups and were subjected to a three-point bend test. The ratio of the measured bending stiffness of the stiffer sample to the more flexible sample was compared with the stiffness ratio predicted by **lam.m**. The results of the two scenarios are presented in Tables 1.

case	Instron load	Matlab load	error	material properties used
[45,-45]; no air gap	11.70 MPa	4.62 Mpa	60.51%	no air gap
[45,-45]; no air gap	11.70 MPa	11.92 Mpa	1.88%	no air gap, w/ -0.002" Sy
[45,-45]; -0.002" air gap	18.25 Mpa	12.13 Mpa	33.53%	-0.002" air gap

case	Instron EI	Matlab EI	error	material properties
stiff / flexible	1.255	1.36	8.37%	no air gap
stiff / flexible	1.255	1.109	11.63%	-0.002" air gap
stiff / flexible	1.255	1.26	0.40%	average

Table 9.1 Instron Results and Matlab predictions.

The material properties referred to in Table 9.1 were found experimentally. In the tension tests, the predicted behavior does not correlate very well with the measured behavior when the correct material properties are used. However, when the tensile strength in the transverse direction with a negative airgap is substituted into the no airgap material properties, the predictive model is quite accurate. Although this substitution seems ungrounded, it has some merit. When the

tensile strength in the transverse direction is measured, the part fails at the weakest of a large number of interfaces. The reported strength is not the average strength between beads but the low end in a Gaussian distribution of strengths. The Matlab program accounts load sharing that occurs by alternating the alignment of the beads, yet it predicts a much lower strength than is found experimentally. This suggests that alternating the alignment of the beads results in an unexpected increase in transverse strength. Additionally, the material exhibits a lot of plastic behavior, something laminated plate theory does not account for. It is possible that the load sharing due to alternating bead alignment coupled with plastic deformation allows the stronger transverse bonds to carry some of the load from the weaker ones, and the part exhibits a transverse strength equal to the mean value of the Gaussian distribution mentioned above.

Because laminated plate theory is intended for brittle elastic materials, it ought to predict the stiffness of an FDM part better than the strength. From Table 1, it is clear that the error in predicting the bending stiffness trends is less than for strengths, for all material properties used. However, the best results are found when the average material properties are used. Again, this suggests that there is some load sharing that we do not understand and is not represented in the Matlab programs. In conclusion, it appears that the principals of laminated plate theory can be applied to FDM parts, but a better understanding of the micro-material properties is needed.

10.0 Build Rules

Based on the results of the experiments performed some build rules have been formulated. These guidelines are intended to aid designers in improving the strength of their parts made on the FDM machine. These rules are listed here with a few illustrative examples of how a rule would apply to a given situation.

Rule 1. *Build parts such that tensile loads will be carried axially along the fibers.*

Figure (10.1) shows a boss along with two cross sections. Two possible orientations for the roads (plastic beads) are shown. In the first cross section, the roads follow the contour of the boss. If a screw were threaded into the boss, the maximum stress (the hoop stress) would be carried axially by the roads going around the contour of the boss. The second cross section is the default orientation that the FDM software would choose. The maximum stress would be carried across the roads in this case.

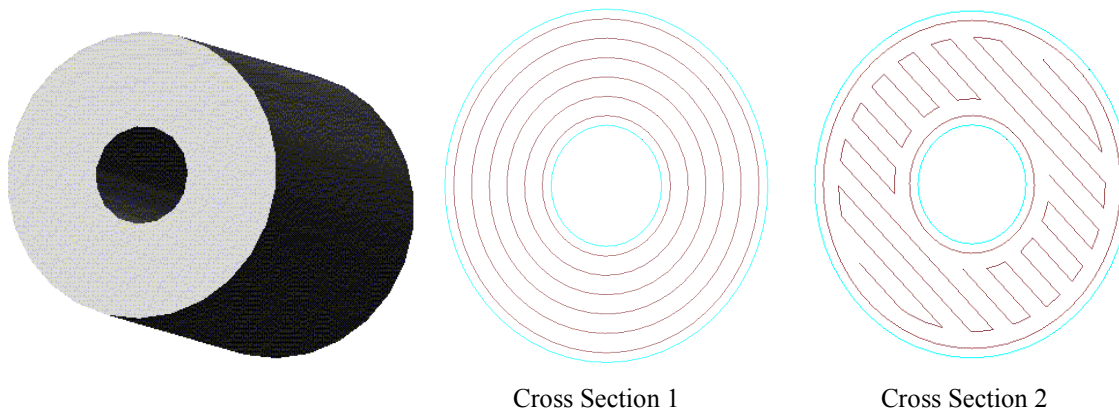


Figure (10.1)

Figure (10.2) shows a cantilever snap fit. Again two different possible build orientations are shown. In the first cross section, the maximum stress (a bending stress in this case) occurs along the roads, while in the second, the maximum stress is carried across the roads. Of course, the snap fit built in the first orientation will be significantly stronger.

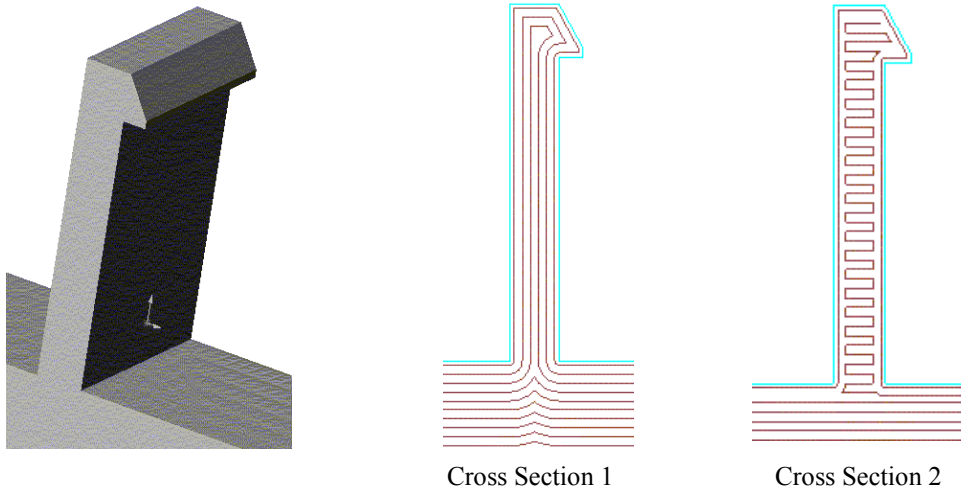


Figure (10.2)

Rule 2: *The stress concentrations associated with a radius can be misleading. If a radius area will carry a load, building the radius with contours is probably best.*

Figure (10.3) shows a standard “dog bone” type tensile specimen which was not used for these tests for reasons already mentioned.

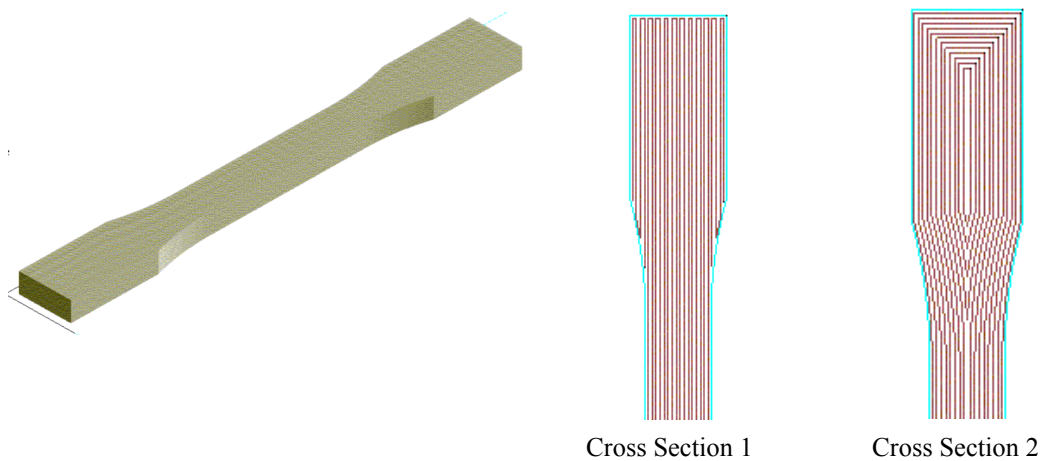


Figure (10.3)

Notice that although the radius is large, there are extreme stress concentrations at the radius in the first cross section. All of the “dog bone” parts that were built and tested in this orientation fractured at the point on the radius where these stress concentrations occur. Cross section 2 shows a better alternative. However, although the stress concentrations along the surface of the radius have been removed, stress concentrations in the center of the part have been created. An additional problem is that the roads are no longer loaded in tension through the radiused part of the specimen. In general, when a radiused area will be carrying a load, it is best to build that radius with contours to alleviate the extreme stress concentrations that can occur.

Rule 3. *A negative air gap increases both strength and stiffness.*

If strength of primary concern, a negative air gap can be used to create a stronger part. However, an air gap less than -0.002 inches should not be used. We found that parts with an air gap less than this simply did not build well due to excess material build up on the nozzle and the part itself. It should be noted that for relatively thick parts, a negative air gap can degrade surface quality and dimensional tolerances.

Rule 4. *Shear strength between layers is greater than shear strength between roads.*

If the part will carry a shear load, try to build is such that the load is carried between layers rather than between roads.

Rule 5. *Bead width and temperature do not affect strength, but the following considerations are important.*

1. Small bead width increases build time.
2. Small bead width increases surface quality.
3. Wall thickness of the part should be an integer multiple of the bead width.

Appendix A

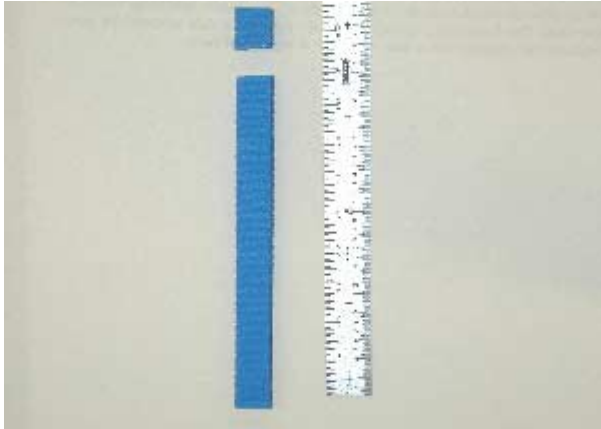


Figure A.1. Tangential (2) failure total rupture.



Figure A.2. Tangential (2) failure: rupture of bond between beads.

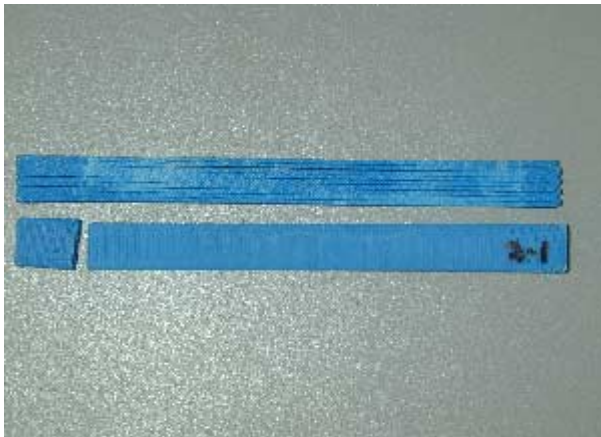


Figure A.3. Elastic vs. plastic failures.

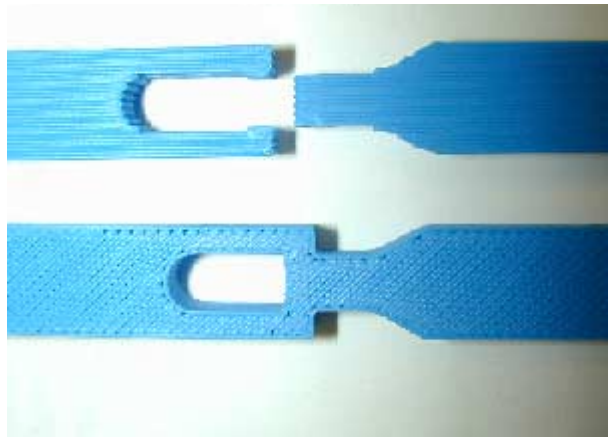


Figure A.4. Shear sample and failure 2 beads ruptured for shear failure



Figure A.5. Tangential (2) failure total rupture at grip.

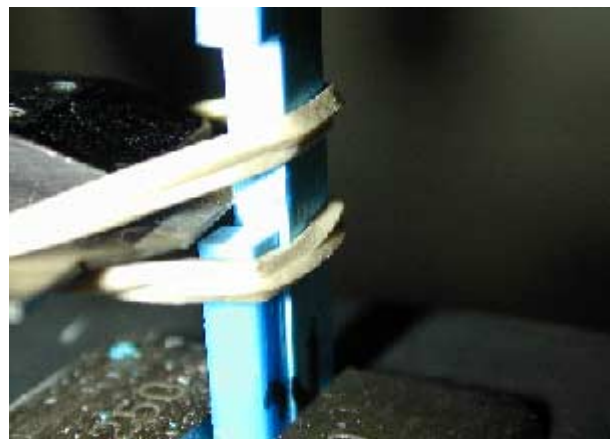


Figure A.6. Axial (1) brittle failure at extensometer blade due to introduction of multi-axial stress and stress concentration.